Synthesis and Characterization of Nearly Monodisperse CdE (E = S, Se, Te) Semiconductor Nanocrystallites

C. B. Murray, D. J. Norris, and M. G. Bawendi*

Contribution from the Department of Chemistry, Massachusetts Institute of Technology, Cambridge, Massachusetts 02139

Received March 22, 1993

Abstract: A simple route to the production of high-quality CdE (E = S, Se, Te) semiconductor nanocrystallites is presented. Crystallites from ~12 Å to ~115 Å in diameter with consistent crystal structure, surface derivatization, and a high degree of monodispersity are prepared in a single reaction. The synthesis is based on the pyrolysis of organometallic reagents by injection into a hot coordinating solvent. This provides temporally discrete nucleation and permits controlled growth of macroscopic quantities of nanocrystallites. Size selective precipitation of crystallites from portions of the growth solution isolates samples with narrow size distributions (<5% rms in diameter). High sample quality results in sharp absorption features and strong "band-edge" emission which is tunable with particle size and choice of material. Transmission electron microscopy and X-ray powder diffraction in combination with computer simulations indicate the presence of bulk structural properties in crystallites as small as 20 Å in diameter.

I. Introduction

The study of nanometer sized crystallites provides an opportunity to observe the evolution of material properties with size. This intermediate size regime is where the collective behavior of bulk materials emerges from the discrete nature of molecular properties. The differing rates with which each of the bulk properties develops provides the possibility of observing and perhaps controlling novel behavior. Nonlinear optical effects from highly polarizable excited states and novel photochemical behavior are two such examples.[1]

The physical properties of semiconductor nanocrystallites are dominated by the spatial confinement of excitations (electronic and vibrational). Quantum confinement, the widening HOMO LUMO gap with decreasing crystallite size, and its implications for the electronic structure and photophysics of the crystallites have generated considerable interest.[1,2] A number of optical studies have begun probing the photoexcited states in such crystallites.[1,2]

Although considerable progress has been made in the controlled synthesis of II–VI semiconductor crystallites,[1,3] interpretation of sophisticated optical experiments often remains difficult due to polydispersities in size and shape, surface electronic defects due to uneven surface derivatization, and poor crystallinity. The study of an appropriate high quality model system is essential in distinguishing properties truly inherent to the nanometer size regime from those associated with variations in sample quality. Each sample must display a high degree of monodispersity (size, shape, etc.), regularity in crystallite core structure, and a consistent surface derivatization (cap).

This paper presents a relatively simple synthetic route to the production of high-quality nearly monodisperse (<5% rms in diameter) samples of CdE (E = S, Se, Te) nanometer size crystallites, with the emphasis on CdSe. The synthesis begins with the rapid injection of organometallic reagents into a hot coordinating solvent to produce a temporally discrete homogeneous nucleation. Slow growth and annealing in the coordinating solvent results in uniform surface derivatization and regularity in core structure. Size selective precipitation provides powders of nearly monodisperse nanocrystallites which can be dispersed in a variety of solvents. The crystallites are slightly prolate with an aspect ratio of 1.1 to 1.3. The average crystallite size, defined by its major axis, is tunable from ~12 to ~115 Å. Room temperature optical absorption and luminescence experiments show that the samples are of high optical quality. Transmission electron microscopy and X-ray powder diffraction are used in combination with computer simulations to characterize nanocrystallite structural features.

II. Experimental Section

General. All manipulations involving alkylcadmium, silylchalconides, phosphines, and phosphine chalconides were carried out using standard airless procedures. Tri-*n*-octylphosphine [TOP] and bis(trimethylsilyl) sulfide [$(TMS)_2S$] were used as purchased from Fluka. Electronic grade (99.99+%) selenium and tellurium shot were purchased from Alfa. Anhydrous methanol, 1-butanol, pyridine, and hexane were purchased from a variety of sources. Tri-*n*-octylphosphine oxide [TOPO] was purchased from Alfa and purified by distillation, retaining the fraction transferred between 260 and 300 °C at ~1 Torr. Dimethylcadmium [Me_2Cd] was purchased from Organometallics Inc. and purified by filtration (0.250 μm) and vacuum transfer. Bis(trimethylsilyl)selenium [$(TMS)_2Se$] and Bis(*tert*-butyldimethylsilyl)tellurium [$(BDMS)_2Te$] were prepared via literature methods[3a,4] and stored at −35 °C in a drybox. Appropriate masses of selenium and tellurium shot were dissolved directly

(1) Recent reviews include: (a) Brus, L. E. *Appl. Phys. A* **1991**, *53*, 465. (b) Henglein, A. *Top. Curr. Chem.* **1988**, *143*, 113. (c) Wang, Y.; Herron, N. *J. Phys. Chem.* **1991**, *95*, 525. (d) Bawendi, M. G.; Steigerwald, M. L.; Brus, L. E. *Annu. Rev. Phys. Chem.* **1990**, *41*, 477.

(2) Recent optical studies include the following: (a) Roussignol, P.; Ricard, D.; Flytzanis, C.; Neuroth, N. *Phys. Rev. Lett.* **1989**, *62*, 312. (b) Alivisatos, A. P.; Harris, A.; Levinos, N.; Steigerwald, M.; Brus, L. E. *J. Chem. Phys.* **1989**, *89*, 4001. (c) Peyghambarian, N.; Fluegel, B.; Hulin, D.; Migus, A.; Joffre, M.; Antonetti, A.; Koch, S. W.; Lindberg, M. *IEEE J. Quantum Electron.* **1989**, *25*, 2516. (d) Bawendi, M. G.; Wilson, W. L.; Rothberg, L.; Carroll, P. J.; Jedju, T. M.; Steigerwald, M. L.; Brus, L. E. *Phys. Rev. Lett.* **1990**, *65*, 1623. (e) Bawendi, M. G.; Carroll, P. J.; Wilson, W. L.; Brus, L. E. *J. Chem. Phys.* **1992**, *96*, 946. (f) Alivisatos, A. P.; Harris, T. D.; Carroll, P. J.; Steigerwald, M. L.; Brus, L. E. *J. Chem. Phys.* **1989**, *90*, 3463. (g) O'Neil, M.; Marohn, J.; McLendon, G. *J. Phys. Chem.* **1990**, *94*, 4356. (h) Eychmuller, A.; Hasserlbarth, A.; Katsikas, L.; Weller, H. *Ber. Bunseges. Phys. Chem.* **1991**, *95*, 79. (i) Wang, Y.; Suna, A.; McHugh, J.; Hillinski, E.; Lucas, P.; Johnson, R. D. *J. Chem. Phys.* **1990**, *92*, 6927. (j) Esch, V.; Fluegel, B.; Khitrova, G.; Gibbs, M.; Jiajin, X.; Chang, S. W.; Koch, S. W.; Liu, L. C.; Risbud, S. W.; Peyghambarian, N. *Phys. Rev. B* **1990**, *42*, 7450. (k) Ekimov, A. I.; Hache, F.; Schanne-Klein, M. C.; Ricard, D.; Flytzanis, C.; Kudryatsev, I. A.; Yazeva, T. V.; Rodina, A. F.; Efros, Al. L. *J. Opt. Soc. Am. B* **1993**, *10*, 100.

(3) (a) Steigerwald, M. L.; Alivisatos, A. P.; Gibson, J. M.; Harris, T. D.; Kortan, R.; Muller, A. J.; Thayer, A. M.; Duncan, T. M.; Douglas, D. C.; Brus, L. E. *J. Am. Chem. Soc.* **1987**, *110*, 3046. (b) Brennan, J. G.; Siegrist, T.; Carroll, P. J.; Stuczynski, S. M.; Brus, L. E.; Steigerwald, M. L. *J. Am. Chem. Soc.* **1989**, *111*, 4141. (c) Spanhel, L.; Haase, M.; Weller, H.; Henglein, A. *J. Am. Chem. Soc.* **1987**, *109*, 5649.

(4) Detty, M. R.; Seidler, M. D. *J. Org. Chem.* **1982**, *47*, 1354.

0002-7863/93/1515-8706$04.00/0

in sufficient TOP to produce 1.0 M stock solutions of trioctylphosphine selenide [TOPSe] and trioctylphosphine telluride [TOPTe].[5]

Method 1. The typical preparation of TOP/TOPO capped CdSe nanocrystallites follows: Fifty grams of TOPO is dried and degassed in the reaction vessel by heating to ~200 °C at ~1 Torr for ~20 min, flushing periodically with argon. The temperature of the reaction flask is then stabilized at ~300 °C under ~1 atm of argon.

Solution A is prepared by adding 1.00 mL (13.35 mmol) of Me_2Cd to 25.0 mL of TOP in the drybox. Solution B is prepared by adding 10.0 mL of the 1.0 M TOPSe stock solution (10.00 mmol) to 15.0 mL of TOP. Solutions A and B are combined and loaded into a 50-mL syringe in the drybox.

The heat is removed from the reaction vessel. The syringe containing the reagent mixture is quickly removed from the drybox and its contents delivered to the vigorously stirring reaction flask in a single injection through a rubber septum. The rapid introduction of the reagent mixture produces a deep yellow/orange solution with an absorption feature at 440–460 nm. This is also accompanied by a sudden decrease in temperature to ~180 °C. Heating is restored to the reaction flask and the temperature is gradually raised to 230–260 °C.

Aliquots of the reaction solution are removed at regular intervals (5–10 min) and absorption spectra taken to monitor the growth of the crystallites. The best quality samples are prepared over a period of a few hours of steady growth by modulating the growth temperature in response to changes in the size distribution as estimated from the absorption spectra. The temperature is lowered in response to a spreading of the size distribution and increased when growth appears to stop. When the desired absorption characteristics are observed, a portion of the growth solution is transferred by cannula and stored in a vial. In this way, a series of sizes ranging from ~15 to 115 Å in diameter can be isolated from a single preparation.

CdTe nanocrystallites are prepared by Method 1 with TOPTe as the chalcogen source, an injection temperature of ~240 °C, and growth temperatures between ~190 and ~220 °C.

Method 2. A second route to the production of CdE (E = S, Se, Te) nanocrystallites replaces the phosphine chalconide precursors in Method 1 with $(TMS)_2S$, $(TMS)_2Se$, and $(BDMS)_2Te$, respectively. Growth temperatures between ~290 and ~320 °C were found to provide the best CdS samples. The smallest (~12 Å) CdS, CdSe, and CdTe species are produced under milder conditions with injection and growth carried out at ~100 °C.

Isolation and Purification of Crystallites. A 10-mL aliquot of the reaction solution is removed by cannula and cooled to ~60 °C, slightly above the melting point of TOPO. Addition of 20 mL of anhydrous methanol to the aliquot results in the reversible flocculation of the nanocrystallites. The flocculate is separated from the supernatant by centrifugation. Dispersion of the flocculate in 25 mL of anhydrous 1-butanol followed by further centrifugation results in an optically clear solution of nanocrystallites and a gray precipitate containing byproducts of the reaction. Powder X-ray diffraction and energy dispersive X-ray analysis indicate these byproducts consist mostly of elemental Cd and Se. This precipitate is discarded. Addition of 25 mL of anhydrous methanol to the supernatant produces flocculation of the crystallites and removes excess TOP and TOPO. A final rinse of the flocculate with 50 mL of methanol and subsequent vacuum drying produces ~300 mg of free flowing TOP/TOPO capped CdSe nanocrystallites. The resulting powder is readily dispersed in a variety of alkanes, aromatics, long-chain alcohols, chlorinated solvents, and organic bases (amines, pyridines, furans, phosphines).

Size-Selective Precipitation. Purified nanocrystallites are dispersed in anhydrous 1-butanol forming an optically clear solution. Anhydrous methanol is then added dropwise to the dispersion until opalescence persists upon stirring or sonication. Separation of supernatant and flocculate by centrifugation produces a precipitate enriched with the largest crystallites in the sample. Dispersion of the precipitate in 1-butanol and size-selective precipitation with methanol is repeated until no further sharpening of the optical absorption spectrum is noted. Size-selective precipitation can be carried out in a variety of solvent/nonsolvent pairs, including pyridine/hexane and chloroform/methanol.

Surface Exchange. Crystallite surface derivatization can be modified by repeated exposure to an excess of a competing capping group. Heating to ~60 °C a mixture of ~50 mg of TOPO/TOP capped crystallites and 5–10 mL of pyridine gradually disperses the crystallites in the solvent. Treatment of the dispersion with excess hexane results in the flocculation of the crystallites which are then isolated by centrifugation. The process of dispersion in pyridine and flocculation with hexane is repeated a number of times to produce crystallites which disperse readily in pyridine, methanol, and aromatics but no longer disperse in aliphatics.

Optical Characterization. Optical absorption spectra were collected at room temperature on a Hewlett-Packard 8452 diode array spectrometer using 1-cm quartz cuvettes. Samples were prepared by dispersing washed CdSe nanocrystallites in hexane. Luminescence experiments were carried out on a SPEX Fluorolog-2 spectrometer with use of front face collection with 500-μm slits. Estimates of quantum yield were obtained by comparing the integrated emission from Rhodamine 640 in methanol and that of 35 Å diameter CdSe nanocrystallites dispersed in hexane. Concentrations of both were adjusted to provide optical densities of 0.30 at 460 nm in matched 1-mm quartz cuvettes. Fluorescence spectra were collected between 480 and 800 nm at room temperature with 460-nm excitation.

Transmission Electron Microscopy. A Topcon EM002B electron microscope operating at 200 kV was used for transmission electron microscopy (TEM). Imaging was carried out in bright field with an objective aperture selected to permit lattice imaging of the (100), (002), and (101) Wurtzite planes. Copper grids (300 mesh) coated with a ~50 Å amorphous carbon film were purchased from Ernest Fullam. Samples were prepared by placing a drop of a dilute pyridine dispersion of nanocrystallites on the surface of a grid, waiting for ~1 min, and then wicking away the solution. The coverage level of crystallites was adjusted by varying the initial dispersion concentration and the contact time.

X-ray Powder Diffraction. Powder X-ray diffraction spectra were collected on a Rigaku 300 Rotaflex diffractometer operating in the Bragg configuration using Cu Kα radiation. The accelerating voltage was set at 250 kV with a 200 milliamp flux. Scatter and diffraction slits of 0.50° and a 0.15-mm collection slit were used. Samples for X-ray diffraction were prepared from ~500 mg of thoroughly washed and dried nanocrystallite powder. The free-flowing powders were pressed at 5000 psi to form 0.5 in. diameter pellets with mirror flat surfaces.

III. Results and Discussion

The production and phenomenology of monodisperse lyophobic colloids has been investigated since Faraday's production of gold sols in 1857.[6] Classic work by La Mer and Dinegar[7] has shown that the production of a series of monodisperse lyophobic colloids depends on a temporally discrete nucleation event followed by controlled growth on the existing nuclei. Temporally discrete nucleation in our synthesis is attained by a rapid increase in the reagent concentrations upon injection, resulting in an abrupt supersaturation which is relieved by the formation of nuclei and followed by growth on the initially formed nuclei.

The work of Steigerwald and co-workers on the use of organometallic precursors in the solution-phase synthesis of bulk and nanocrystalline materials provides guidance in our selection of reagents.[3a,b,8] Me_2Cd is chosen as the Cd source and $(TMS)_2E$ (E = S, Se, Te) or TOPSe and TOPTe are selected as chalcogen sources with TOPSe and TOPTe preferred due to their ease of preparation and their stability. Me_2Cd and $(TMS)_2E$ reagents have been shown to undergo dealkylsilylation in a variety of solvents as a route to the production of bulk materials.[8] Trimethylphosphine telluride is known as a good source of Te^0.[9] Mixed phosphine/phosphine oxide solutions have previously been found to be good solvents for the high-temperature growth and annealing of CdSe crystallites.[2d,e,10] The coordinating solvent plays a crucial role in controlling the growth process, stabilizing the resulting colloidal dispersion, and electronically passivating the semiconductor surface.

Nucleation and Growth. Injection of reagents into the hot reaction pot results in a short burst of homogeneous nucleation.

(5) Zingaro, R. A.; Steeves, B. H.; Irgorlic, K. *J. Organomet. Chem.* **1965**, *4*, 320.

(6) Overbeek, J. Th. G. *Adv. Colloid Interface Sci.* **1982**, *15*, 251.

(7) LaMer, V. K.; Dinegar, R. H. *J. Am. Chem. Soc.* **1950**, *72*, 4847.

(8) Stuczynski, S. M.; Brennan, J. G.; Steigerwald, M. L. *Inorg. Chem.* **1989**, *28*, 4431.

(9) (a) Steigerwald, M. L.; Sprinkle, C. R. *J. Am. Chem. Soc.* **1987**, *109*, 7200. (b) Steigerwald, M. L. *Chem. Mater.* **1989**, *1*, 52.

(10) Bawendi, M. G.; Kortan, A. R.; Steigerwald, M. L.; Brus, L. E. *J. Chem. Phys.* **1989**, *91*, 7282.

The depletion of reagents through nucleation and the sudden temperature drop associated with the introduction of room temperature reagents prevents further nucleation. Gently reheating allows slow growth and annealing of the crystallites. Crystallite growth appears consistent with "Ostwald ripening", where the higher surface free energy of small crystallites makes them less stable with respect to dissolution in the solvent than larger crystallites. The net result of this stability gradient within a dispersion is slow diffusion of material from small particles to the surface of larger particles.[11] Reiss has shown how growth by this kind of transport can result in the production of highly monodisperse colloidal dispersions from systems that may initially be polydisperse.[12]

Both the average size and the size distribution of crystallites in a sample are dependent on the growth temperature, consistent with surface free energy considerations. The growth temperature necessary to maintain steady growth increases with increasing average crystallite size. As the size distribution sharpens, the reaction temperature must be raised to maintain steady growth. Conversely, if the size distribution begins to spread, the temperature necessary for slow steady growth drops. Size distributions during growth are crudely estimated from absorption line widths (typically 50 nm fwhm). Modulation of the reaction temperature in response to changes in the absorption spectrum allows the maintenance of a sharp size distribution as the sample grows.

The Ostwald ripening process accentuates any kinetic or thermodynamic "bottleneck" in the growth of crystallites. As a bottleneck is approached (e.g. a closed structural shell), sharpening of the sample size distribution reduces the thermodynamic driving force for further growth. Sharpening in the absorption features as the average particle size approaches 12, 20, 35, 45, and 51 Å in diameter may point to the presence of such bottlenecks.

Capping groups present a significant steric barrier to the addition of material to the surface of a growing crystallite, slowing the growth kinetics. The TOP/TOPO solvent coordinates the surface of the crystallites and permits slow steady growth at temperatures above 280 °C. Replacing the octyl chains with shorter groups reduces the temperature for controlled growth. Mixed alkylphosphine/alkylphosphine oxide solvents with butyl, ethyl, and methyl groups show uncontrolled growth at 230, 100, and 50 °C, respectively. Steady controlled growth results in highly monodisperse particles of consistent crystal structure and allows size selection by extracting samples periodically from the reaction vessel.

A wealth of potential organometallic precursors and high boiling point coordinating solvents exist. Although phosphine/phosphine oxide have been found to provide the most controlled growth conditions, injections of reagents into hot pyridines, tertiary amines, and furans all allow production of nanocrystallites.

We are beginning the extension of this synthetic method to the production of ZnE and HgE materials using diethylzinc and dibenzylmercury as group II sources. Growth conditions have not yet been optimized to provide sample quality comparable to that of CdE materials.

Colloid Stabilization and Size-Selective Precipitation. Lyophobic colloidal particles attract each other by van der Waals forces. The attraction is strong due to the near additivity of forces between pairs of unit cells in different particles.[13] Colloids remain stable with respect to aggregation only if there exists a repulsive force of sufficient strength and range to counteract the van der Waals attraction. Chemisorption of ambiphylic species on the surface of the particles gives rise to a steric barrier to aggregation. The dispersions of CdSe nanocrystallites are sterically stabilized by a lyophylic coat of alkyl groups anchored to the crystallite surface by phosphine oxide/chalconide moieties. The efficiency of the steric stabilization is strongly dependent on the interaction of the alkyl groups with the solvent. Gradual addition of a nonsolvent can produce size-dependent flocculation of the nanocrystallite dispersion. This phenomenon is exploited in further narrowing the particle size distribution.

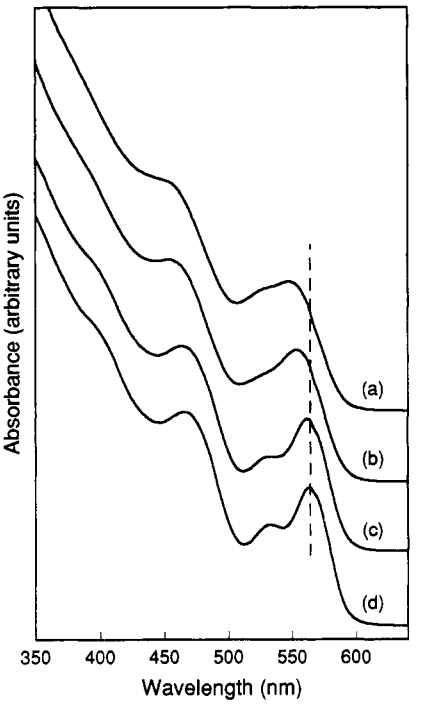

Figure 1. Example of the effect of size-selective precipitation on the absorption spectrum of ~37 Å diameter CdSe nanocrystallites. (a) Room temperature optical absorption spectrum of the nanocrystallites in the growth solution before size-selective precipitation. (b) Spectrum after one size-selective precipitation from the growth solution with methanol. (c) Spectrum after dispersion in 1-butanol and size-selective precipitation with methanol. (d) Spectrum after a final size-selective precipitation from 1-butanol/methanol.

The addition of methanol increases the average polarity of the solvent and reduces the energetic barrier to flocculation. The largest particles in a dispersion experience the greatest attractive forces. These large particles have a higher probability of overcoming the reduced barrier and are thus enriched in the flocculate produced. The removal of a specific subset of particles from the initial size distribution narrows the size distribution of both supernatant and precipitate. Depending on the cap molecule, a number of solvent/nonsolvent systems can be used for size-selective precipitation (e.g. hexane/ethanol, chloroform/methanol, pyridine/hexane, etc....).

Figure 1 illustrates the result of size-selective precipitation. Spectrum a shows the optical absorption of the initial growth solution. The broad absorption features correspond to a sample with an average size of 35 Å ± 10% (sized by TEM). Slow addition of methanol results in the flocculation of the larger particles in the distribution which give spectrum b after dispersing in 1-butanol. Titration of methanol in sample b again produces flocculation of the larger particles, giving spectrum c upon dispersion in 1-butanol. A final size-selective precipitation from 1-butanol yields a sample with optical absorption d and with an average size of ~37 Å ± 5%. Spectrum d is dramatically sharpened relative to that of the initial growth solution and reveals transitions at 530 and ~400 nm which were previously cloaked by polydispersity. For the fractionation process to work well it is crucially important that the shape and surface derivatization of the initial crystallites be uniform and that the initial polydispersity in size be relatively small.

(11) Smith, A. L. *Particle Growth in Suspensions*; Academic Press: London, 1983; pp 3–15.
(12) Reiss, H. *J. Chem. Phys.* **1951**, *19*, 482.
(13) Sato, T.; Ruch, R. *Stabilization of Colloidal Dispersions by Polymer Absorption*; Marcel Dekker: New York, 1980; pp 46–51.

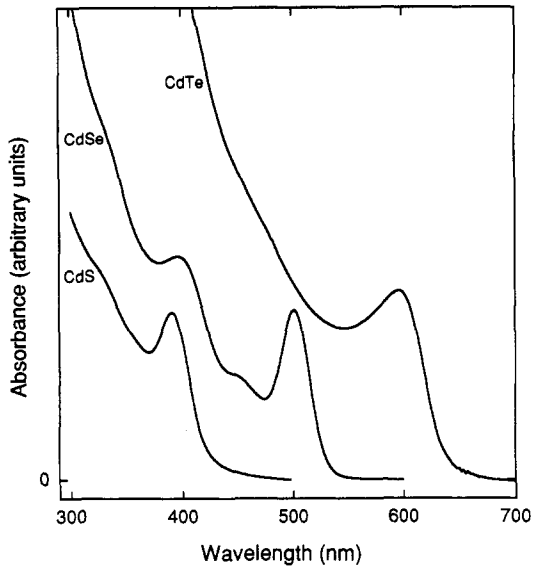

Figure 2. Room temperature optical absorption spectra of ~20–30 Å diameter CdS, CdSe, and CdTe crystallites.

Surface Exchange. Preliminary studies of surface exchange have been used to tailor the compatibility of crystallites with a variety of solvents. Exposure of purified crystallites to a large excess of pyridine begins the exchange of the surface cap. Addition of solvents compatible with TOPO and TOP but incompatible with the new cap results in the flocculation of the crystallites and the removal of displaced TOP and TOPO species. The repeated dispersion in pyridine and isolation with alkanes drives the surface exchange with mass action. Crystallites capped with pyridine are dispersible in polar solvents and aromatics but not aliphatics. Surface exchange results in a slight decrease in average crystallite size and a small broadening of the size distribution, probably due to the loss of species containing Cd and Se. Sharp optical features can be recovered by size-selective precipitation from pyridine with the titration of hexane. Crystallites can be stabilized in a variety of solvents with a range of functionalized caps. There is obvious potential for customizing photochemical activity of these robust chromophores through manipulation of their immediate chemical environment.

Optical Properties. The absorption spectra of ~20–30 Å diameter CdS, CdSe, and CdTe nanocrystallite samples are shown in Figure 2. All three clearly show the effect of quantum confinement. CdS, CdSe, and CdTe absorptions are shifted dramatically from their 512, 716, and 827 nm bulk band gaps, respectively. The CdSe spectrum shows three clearly resolved transitions while the CdS and CdTe samples show less structure. We do not believe the difference in quality of the optical spectra reflects any fundamental material limitations but rather the amount of effort spent in optimizing the growth conditions for each material.

Figure 3 shows the evolution of the optical spectrum with size in a series of room temperature absorption spectra for CdSe crystallites ranging from ~12 to 115 Å in diameter. The series spans a range of sizes from nearly molecular species containing fewer than 100 atoms to fragments of the bulk lattice containing more than 30 000 atoms. Figure 4 compares the experimentally observed HOMO LUMO gap as a function of particle size with the prediction of the simple effective mass approximation with the Coulomb interaction treated in first-order perturbation.[1d] All particle sizes were determined by TEM and confirmed by X-ray line-shape analysis. Although experiment and theory agree reasonably well at large sizes, the simple theory diverges from the experimental values for small sizes as expected from the non-parabolicity of the bands at higher wave vectors and the finite potential barrier at the surface of the particles. Lippens and

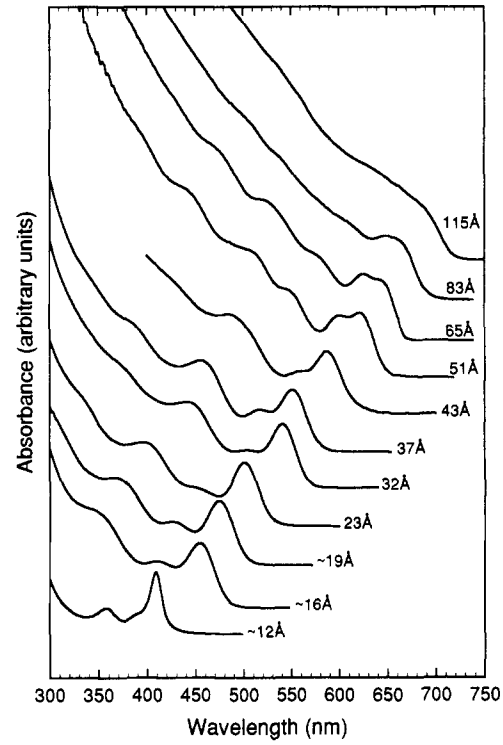

Figure 3. Room temperature optical absorption spectra of CdSe nanocrystallites dispersed in hexane and ranging in size from ~12 to 115 Å.

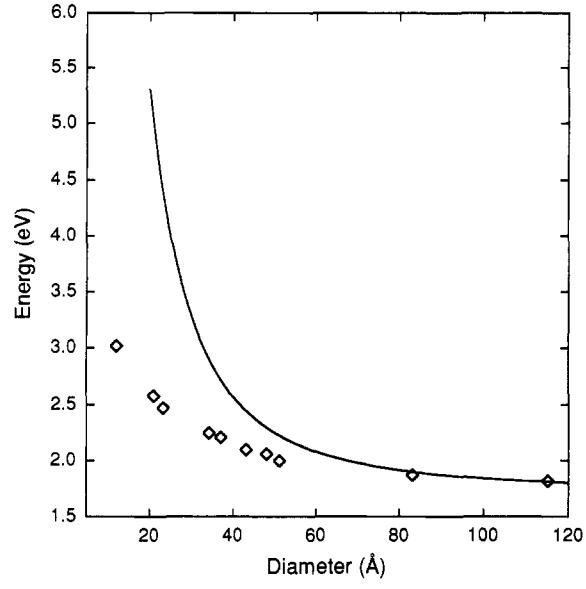

Figure 4. HOMO LUMO transition energy of CdSe crystallites as a function of size (diamonds) compared with the prediction of the effective mass approximation (solid line).

Lannoo[14] have shown that tight binding calculations can yield better agreement for these smaller sizes.

Figure 5 shows the room temperature photoluminescence spectrum of a sample of 35 Å diameter CdSe crystallites and compares it with the absorption spectrum. The luminescence quantum yield for this sample is ~9.6% relative to Rhodamine 640 at room temperature. The line width in emission is equal to that in absorption, with the peak of the emission shifted 4 nm to the red of the absorption maximum. This shift is the result of a combination of relaxation into shallow trap states and the size distribution.[2e] No deep trap emission was detected.

(14) (a) Lippens, P. E.; Lannoo, M. *Phys. Rev. B* **1989**, *39*, 10935. (b) Lippens, P. E.; Lannoo, M. *Mater. Sci. Eng. B* **1991**, *9*, 485.

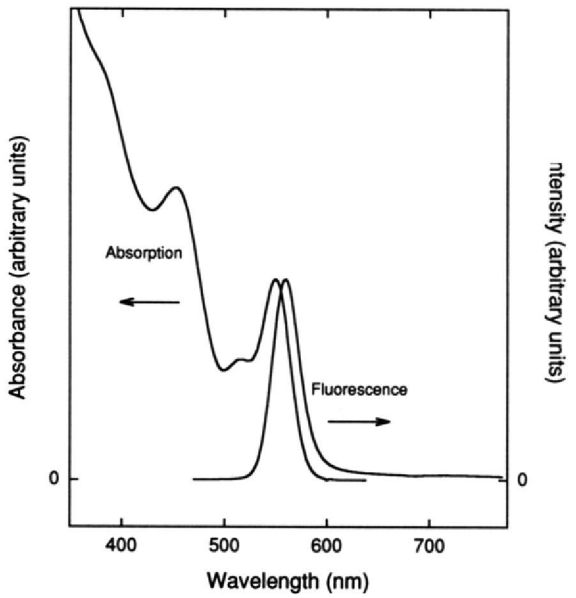

Figure 5. Typical room temperature band edge luminescence and absorption spectra for 35 Å diameter CdSe crystallites. No deep trap luminescence is detected.

The sharp absorption features suggest highly monodisperse samples. High quantum yields and narrow emission line widths indicate growth of crystallites with few electronic defect sites. The sharp luminescence is a dramatic example of the efficiency of the capping group in electronically passivating the crystallites. The capping groups also protect the individual crystallites from chemical degradation yielding robust systems. Samples stored in the original growth solution still show strong, sharp emission after storage for more than a year.

These room temperature optical experiments, carried out on common laboratory equipment, demonstrate the benefits of high-quality samples and point to the potential of more sophisticated optical studies on these samples.

Transmission Electron Microscopy. Transmission electron microscopy allows imaging of individual crystallites and the development of a statistical description of the size and shape of the particles in a sample. High magnification imaging with lattice contrast allows the determination of individual crystallite morphology.[15]

Imaging at 590×10^3 times magnification with moderate crystallite coverage allows careful size measurements of 30 to 50 individual nanocrystallites on a single image and shows that the particles are not aggregated. Figure 6 shows a collection of slightly prolate CdSe nanocrystallites averaging 35 Å ± 5% in the direction of the (002) wurtzite axis and 30 Å ± 6% perpendicular to the (002) axis. Particles with the (002) axis perpendicular to the grid are identified by a characteristic hexagonal pattern in atom imaging and are nearly circular in cross section. Particles oriented in other directions appear slightly oblong. The analysis of samples ranging from ~20 up to 115 Å indicates slightly prolate particles with aspect ratios between 1.1 and 1.3.[16] Samples generally have standard deviations <5% in the long axis and <6% in the shorter dimension. All diameters quoted in this paper are a measure of the major axis. This axis is more precisely measured because it is easier to distinguish the edge of a crystallite in the (002) direction rather than perpendicular to it. The loss of contrast at the surface of the crystallite makes the assignment of the final atomic plane uncertain and introduces the greatest source of experimental error. The standard deviation values are thus actually measurement limited with an experimental uncertainty of one atomic plane per crystallite.

(15) Kihilborg. L. *Prog. Solid State Chem.* **1990**, *20*, 101.
(16) Similar aspect ratios have been previously observed. See: Rossetti, R.; Ellison, J. L.; Gibson, J. M.; Brus, L. E. *J. Chem. Phys.* **1984**, *80*, 4464.

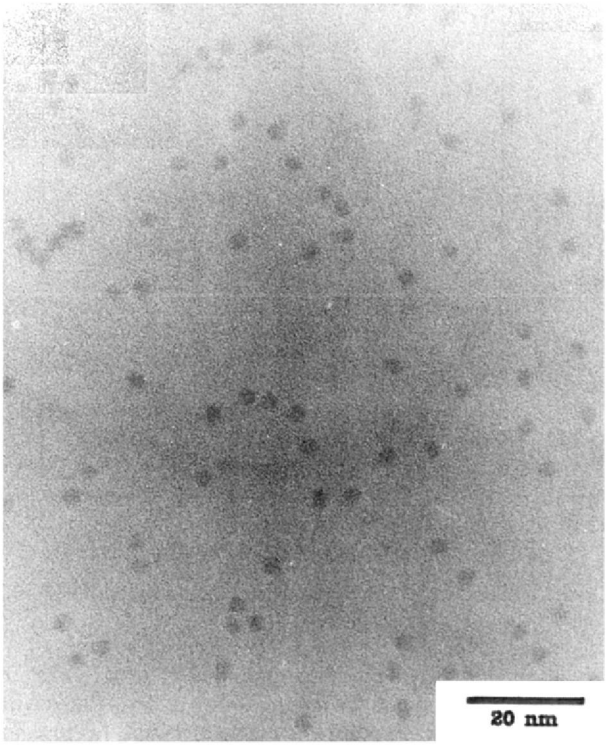

Figure 6. TEM image taken in bright field with lattice contrast shows a collection of slightly prolate particles. The elongated (002) axis measures 35.0 Å ± 5% while the perpendicular axis measures 30 Å ± 6%. The particles are well dispersed and not aggregated.

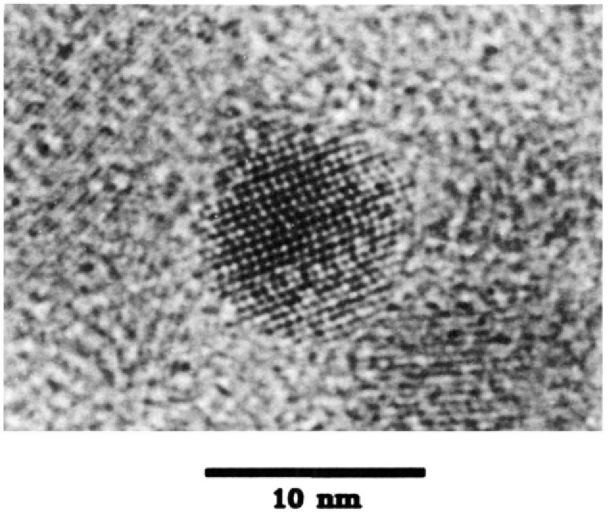

Figure 7. An 80 Å diameter CdSe crystallite imaged in bright field with atom contrast shows the presence of stacking faults in the (002) direction.

High-magnification imaging (590×10^3 to 1×10^6) allows the detection of planar disorder in individual crystallites. Figure 7 shows an 80 Å diameter CdSe nanocrystallite atom imaged perpendicular to the (100) and (002) axes. Planar disorder along the (002) axis is clearly observed. Figure 8 shows a ~110 Å diameter crystallite with a 1.33 aspect ratio and four clear stacking faults in the (002) direction (the left particle). A neighboring crystallite displays the hexagonal atom imaging pattern resulting from imaging along the (002) axis. No planar disorder is detectable in this projection. The analysis of a series of samples leads to some general results. The (002) planes (perpendicular to the long axis) show little disorder while loss of lattice image contrast is most commonly seen in the (100) planes (parallel to the long axis) and in the (101) planes. This loss of contrast is believed to result from the presence of stacking faults along the (002) direction. These stacking faults are the predominant form

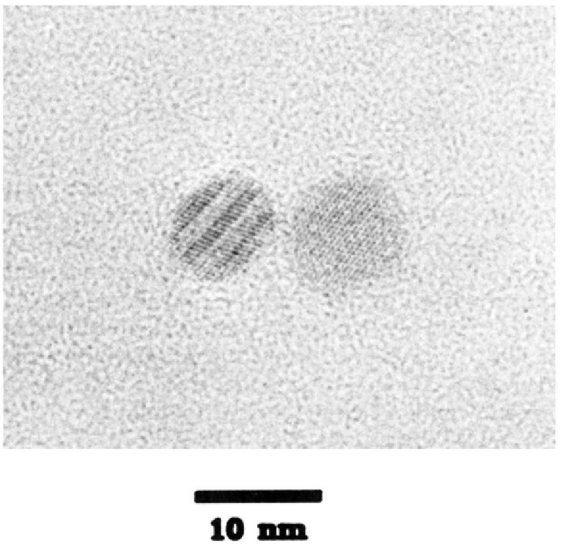

Figure 8. The crystallite on the left (~110 Å) shows a loss of lattice contrast in the (101) planes pointing to the presence of 4 stacking faults along the (002) direction. The crystallite is prolate with an aspect ratio of ~1.3. The crystallite on the right presents a projection perpendicular to the (002) direction and displays the hexagonal atom imaging characteristics of the wurtzite structure.

of disorder in bulk II–VI materials.[17a] Chaderton *et al.* also use changes in lattice contrast to identify individual stacking faults in a series of 100-nm II–VI thin films.[18]

There is a broad distribution in the position and frequency of stacking faults within each sample. Statistically more stacking faults are observed near the center of crystallites which may point to an increased probability of faulting early in the growth. It is also possible that greater contrast in the central region improves the detection of faults. The wavy lattice patterns of individual faulted crystallites seen in TEM can be qualitatively reproduced in computer generated atom images of crystallites by introducing stacking faults along the (002) axis.

TEM allows not only the investigation of the morphology of individual crystallites but also the observation of ordering of crystallites into secondary structures. Two-dimensional hexagonal close packing begins to form (Figure 9) at relatively high coverage levels. The tailoring of mixed solvents in the fashion permitting selective precipitation may allow more controlled growth of such secondary structures.

Selected area electron diffraction patterns confirm a predominantly wurtzite structure. Although a common technique, selected area diffraction is not emphasized in our structural analysis. Bright field images indicate that our crystallites are not randomly oriented on the TEM grid but exhibit a tendency to orient with their long axis parallel to the carbon surface. The nonstatistical distribution of crystal orientations can greatly impair the interpretation of electron diffraction line shapes. Electron microdiffraction may provide an appropriate alternative to selected area diffraction in these systems.[19]

X-ray Diffraction. Unlike TEM, X-ray powder diffraction probes a large number of crystallites that are statistically oriented. Samples are prepared as dense pellets free of any amorphous binder to provide a strong signal with low background. The pellets disperse readily in a variety of solvents with no apparent change in the absorption spectra.

Samples of CdS, CdSe, and CdTe crystallites all exhibit a predominantly wurtzite crystal structure with the lattice spacing

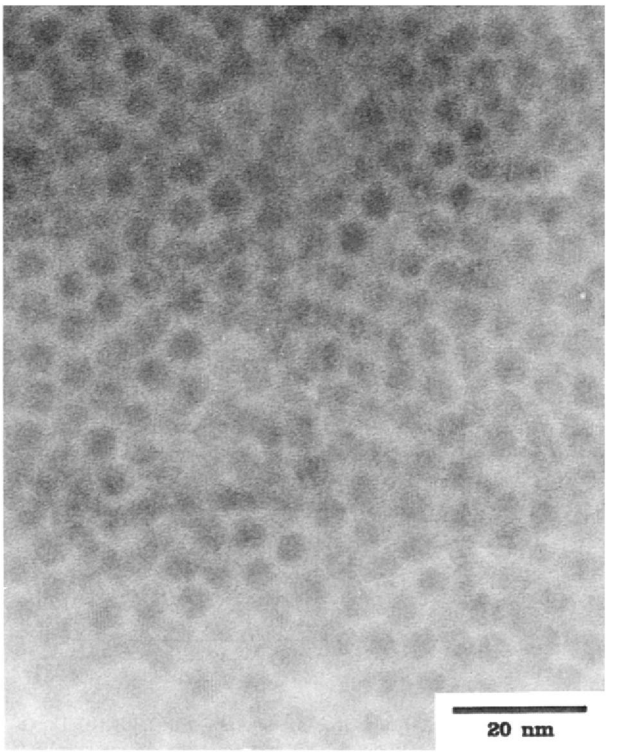

Figure 9. A near monolayer of 51 Å diameter CdSe crystallites showing short-range hexagonal close packing.

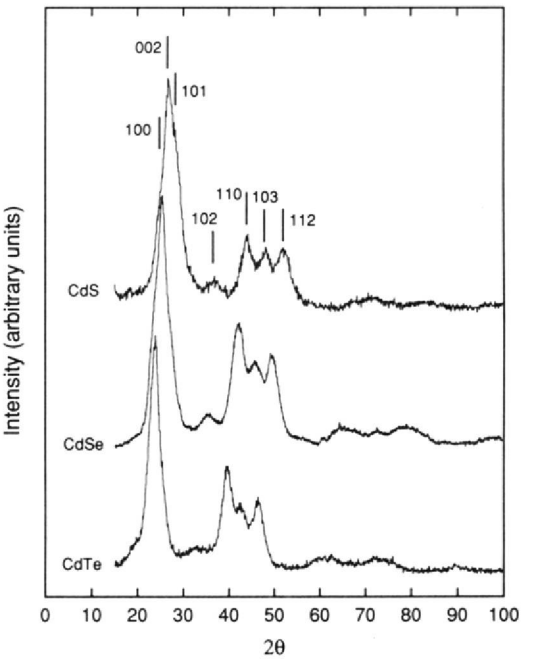

Figure 10. Powder X-ray diffraction spectra of ~35 Å CdS, CdSe, and CdTe crystallites. The positions of bulk reflections for wurtzite CdS are indicated.

of the bulk materials (Figure 10). Bulk crystals of CdS and CdSe commonly exhibit the wurtzite structure when prepared at high temperature. The hexagonal modification of CdTe has been observed in thin films although to our knowledge it has not been seen in bulk crystals.[17b]

Experimental X-ray powder diffraction spectra for CdSe crystallites ranging from ~12 to 115 Å in diameter are displayed in Figure 11. Spectra show evidence of finite size broadening in all reflections.[20a] Excessive attenuation and broadening in the

(17) Aven, M.; Prener, J. S. *Physics and Chemistry of II–VI Compounds*; North Hollond: Amsterdam, 1967; pp 144 (a) and 132 (b).
(18) Chadderton, L. T.; Fitzgerald, A. G.; Yoffe, A. D. *Nature* **1963**, *198*, 573.
(19) Loretto, M. H. *Electron beam analysis of Materials*; Chapman and Hall: London, 1984; pp 50–53.
(20) Guinier, A. *X-Ray Difrraction*; W. H. Freeman: San Francisco, 1963; pp 122–149 (a) and 226–237 (b).

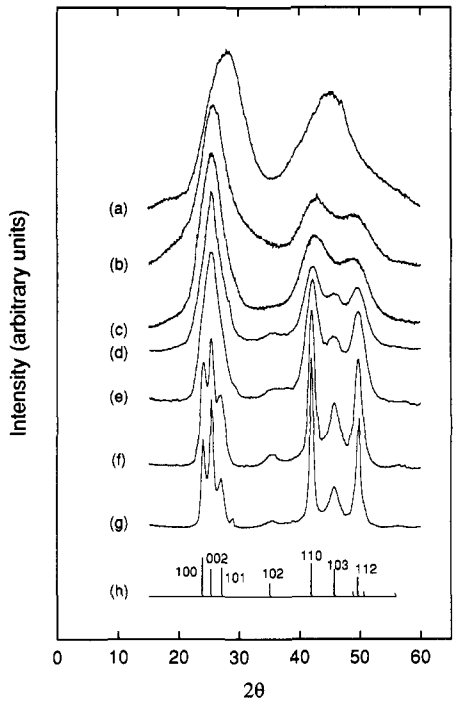

Figure 11. Powder X-ray diffraction spectra of (a) 12, (b) 18, (c) 20, (d) 37, (e) 42, (f) 83, and (g) 115 Å diameter CdSe nanocrystallites compared with the bulk wurtzite peak positions (h).

(102) and (103) reflections are characteristic of stacking faults along the (002) axis.[20b] The diffraction pattern of the ~12 Å diameter species appears dramatically different from that of the other sizes. These small clusters possess too few atoms to define a core crystal structure, making the distinction between wurtzite and zincblende meaningless. The dramatic change in their diffraction features may indicate significant surface reconstruction or contributions from the capping groups to the diffraction pattern. Proper structural analysis of these nearly molecular species will require the isolation of materials as single crystals as has been achieved with CdS.[21]

Structural Simulations. Modeling of nanocrystallite samples as collections of monodisperse spherical single crystals with ideal surface termination is appealing but may potentially be misleading. In this section we develop a working description of average crystallite morphology using a combination of experimental and computer simulated X-ray diffraction patterns and parameters which are consistent with other independent structural probes.

The combination of finite size and defect broadening results in a convolution of peaks in the X-ray diffraction spectra. Direct observation of peak positions and peak widths are thus unreliable measures of lattice spacing and crystallite size. But structural information can be extracted by using TEM and EXAFS[22] observations to guide in fitting the experimental X-ray diffraction spectra. Previous studies of the X-ray powder patterns of CdSe nanocrystallites have demonstrated the sensitivity of spectra to the presence of planar disorder and thermal effects.[10] These studies are extended here over a range of sizes. The importance of crystallite shape, the question of lattice contractions, and probable surface disorder are investigated.

(21) Herron, N.; Calabrese, J. C.; Farneth, W. E.; Wang, Y. *Science* **1993**, *259*, 1426. Our smallest CdS particles have optical spectra identical with those in this reference. We believe the smallest CdSe particles in our series are the CdSe analogue to the CdS particles crystallized in this work.

(22) (a) Marcus, M. A.; Flood, W.; Steigerwald, M. L.; Brus, L. E.; Bawendi, M. G. *J. Phys. Chem.* **1991**, *95*, 1572. (b) Marcus, M. A.; Brus, L. E.; Murray, C. B.; Bawendi, M. G.; Prasad, A.; Alivisatos, A. P. *Nanostruct. Mater.* **1992**, *1*, 323.

Fits to experimental spectra employ a discrete form of the Debye equation,[23]

$$I(S) = I_0 \frac{f^2(S)}{2\pi S} \sum_k \frac{p(r_k)}{r_k} \sin(2\pi r_k S)$$

where $I(S)$ is the diffracted intensity, I_0 is the incident intensity, $f(S)$ is the scattering factor, and S is the scattering parameter [$S = 2 \sin(q)/\lambda$ for X-rays of wavelength λ diffracted through angle q]. The sum is over all discretized interatomic distances r_k, and $p(r_k)$ is the number of times a given interatomic distance r_k occurs. Since the number of discrete interatomic distances in an ordered structure grows much more slowly than the total number of distances, the discrete form of the equation is significantly more efficient for large crystallites.

Atomic coordinates are obtained by systematically generating atomic positions for a bulk crystalline lattice and retaining only those atoms falling within a defined ellipsoid. EXAFS studies[22] support the use of bulk bond lengths (2.63 Å for CdSe). The dimensions for the ellipsoid are taken from TEM measurements of average size and shape. Planar disorder along the (002) axis is reproduced by creating a collection of coordinate files with a broad distribution of stacking faults about the center of the crystallites. The resulting spectra are statistically weighted and summed to create a crystallite sample distribution with a defined average defect density. Thermal effects are simulated by the introduction of a Debye–Waller factor.[24] A constant Debye–Waller factor is used based on a mean-square displacement of 0.04 Å^2 for each atom, consistent with EXAFS studies[22] which find bulk Debye–Waller factors. The Debye–Waller factor does not change peak positions and only affects peak intensities through an exponential damping as 2θ increases. The broad backgrounds in the experimental diffraction spectra are subtly influenced by the combined effects of experimental geometry, variable absorption of X-rays, contributions from incoherent scattering, thermal effects (Debye–Waller term), and scattering from the capping groups. Rigorous correction of the background from these contributions requires a knowledge of sample properties not presently available. A constant background chosen to best fit the relative intensity of the (110) reflection for 37 Å crystallites is added to all simulated spectra to crudely compensate for the experimental contributions to the background. This background is not important in our analysis which concentrates on the diffraction features.

Figure 12 compares calculated spectra of 1000 atom spherical CdSe particles (~37 Å diameter) with the experimental powder pattern of a similarly sized sample. The spectra of defect free zincblende (a) and wurtzite (b) crystallites do not reproduce the overall shape of experimental spectrum d, especially in the region between the (110) and (112) peaks. The introduction of a single stacking fault near the center of an otherwise wurtzite crystallite greatly improves the fit (spectrum c) by broadening the (103) peak.

The (110) spacing is present in both the wurtzite and zincblende structures and is thus unaffected by the presence of stacking faults along the (002) axis. This spacing also has reasonable separation from neighboring reflections. Crude estimates of particle size based on the Scherer analysis of peak widths should employ the width of the (110) feature rather than the convolution of the (100), (002), and (101) reflections found in the first diffraction feature. This convolution is easily confused with the (111) zincblende reflection, and using it to estimate particle size would underestimate the coherence length. The agreement in the width and shape of the (110) feature between our simulated spectra using crystallite dimensions based on TEM measurements

(23) Hall, B. D.; Monot, R. *Comput. Phys.* **1991**, *5*, 414.

(24) Vetelino, J. F.; Guar, S. P.; Mitra, S. S. *Phys. Rev. B* **1972**, *5*, 2360.

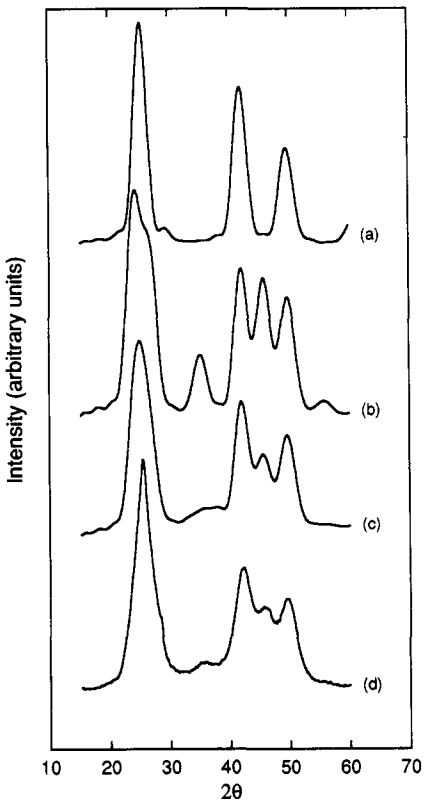

Figure 12. Simulated X-ray powder diffraction spectra for 35 Å diameter spherical nanocrystallites: (a) pure zincblende, (b) pure wurtzite, (c) wurtzite with one stacking fault. (d) Experimental powder spectrum of ~35 Å diameter crystallites.

and our experimental spectra confirms crystallite size and indicates that structural defects must be coherent defects (e.g. stacking faults).

Figure 13 highlights the sensitivity of the diffraction spectrum to crystallite shape. The experimental spectrum of a sample of CdSe nanocrystallites containing on average ~10 000 atoms (~80 Å diameter) is compared with simulations. The best fits obtained assuming spherical particles (spectrum a) and prolate particles with an aspect ratio of 1.3 in the (002) direction (spectrum b) are shown. Each simulation has an average defect density of 3 stacking faults per crystallite to fit the region of the (103) peak. While the (100) feature is more intense than the (002) peak in bulk CdSe and in the simulated spectrum of spherical particles, the opposite is true for our crystallites and in the simulation of prolate particles. The elongated particles have a larger number of (002) planes, making that peak the dominant reflection in the first diffraction feature. The greater coherence length in that direction results in the narrowing of (002) reflection and a smaller overlap with the neighboring(100) and (101) reflections. Inclusion of the prolate nature of the particles, observed in TEM, is essential for reproducing the shape of the convolution of the (100), (002), and (101) reflections. We fix the aspect ratio at ~1.3 for the simulations of the other sizes to minimize the number of floating parameters.

The first broad diffraction feature ($2\theta \sim 25°$) appears to shift to higher scattering angles with decreasing particle size (Figure 11). An isotropic lattice contraction of a few percent due to surface tension has been proposed as a possible explanation for similar observations in CdS nanocrystallites.[25] EXAFS data[22] however yield average bond lengths which are essentially identical with those in the bulk even for the smallest crystallites. In fact, even the small ~12 Å CdS clusters recently crystallized by Herron et al.[21] only show a bond contraction of ~0.5% compared to the bulk. This apparent contradiction can be resolved in our samples by properly taking crystallite shape into account. Figure 14a compares the experimental spectrum of small CdSe crystallites containing ~275 atoms (~20 Å diameter) to the simulated spectrum of spherical particles with a bulk lattice parameter, showing a clear shift of the first experimental peak to higher angles. Figure 14b compares the same experimental spectrum with the simulated spectrum of spherical particles with a lattice

(25) (a) Wang, Y.; Herron, N. *Phys. Rev. B* **1990**, *42*, 7253. (b) Goldstein, A. N.; Echer, C. M.; Alivisatos, A. P. *Science* **1992**, *256*, 1425. (c) Colvin, V. L.; Goldstein, A. N.; Alivisatos, A. P. *J. Am. Chem. Soc.* **1992**, *114*, 5221.

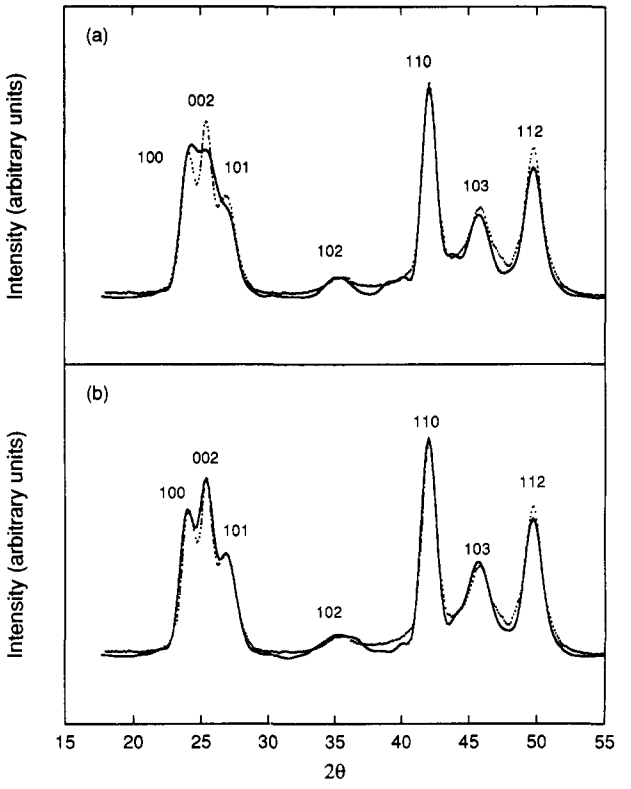

Figure 13. Experimental X-ray powder diffraction spectrum of ~80 Å diameter (~10 000 atoms) crystallites (dotted line) compared with computer simulations (solid line) of (a) spherical and (b) prolate particles [aspect ratio of 1.3 along the (002) direction]. Three stacking faults on average and bulk lattice constants are used.

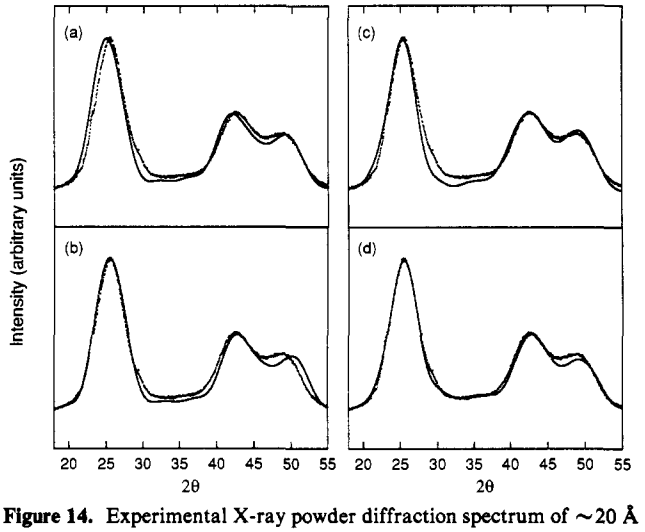

Figure 14. Experimental X-ray powder diffraction spectrum of ~20 Å (~275 atoms) diameter crystallites (dotted line) compared with a series of computer simulations of wurtzite crystallites containing 275 atoms with one stacking fault per crystallite in the (002) direction (solid lines). (a) Spherical particles with bulk lattice parameters, (b) spherical particles with a 2% isotropic lattice contraction, (c) prolate particles [aspect ratio of 1.3 along the (002) axis] with bulk lattice parameter, (d) moderate surface disorder added to the prolate particles of part c.

parameter contracted by 2%. A constant defect density of one stacking fault/crystallite is used in both simulations to fit the valley between the (110) and (112) peaks. The 2% contraction is designed to reproduce the position and general shape of the first diffraction feature but results in a poor fit at higher angles. Observation of a shift in the first peak is not enough to prove a lattice contraction. The higher peaks must also shift. Figure 14c shows the effect of putting an aspect ratio on the crystallites. The experimental pattern is compared with the simulated spectrum of prolate particles having an aspect ratio of ~1.3 in the (002) direction, a bulk lattice parameter, and one stacking fault per crystallite. The introduction of crystallite shape uniformly improves the fit without requiring a major lattice contraction. The prolate shape results in the prominence of the (002) reflection, skewing the first diffraction feature to higher scattering angles. This effect is especially important for smaller crysatllites which have few planes and where a single extra plane has a tremendous effect on the intensity and width of the diffraction feature for that direction. Thus, for the same aspect ratio, small crystallites exhibit a larger apparent shift than larger crystallites. Fits with prolate crystallites reproduce the position of the peaks and the general shape of the spectrum but show a lack of intensity in a broad region between $2\theta \sim 27°$ and 33° compared to the experimental data.

TEM observations suggest poorly resolved facets and the presence of a potentially reconstructured surface layer limiting the accuracy of measurements to no better than one atomic plane. The presence of surface disorder is simulated in our studies by the relaxation of all atoms lacking their full coordination shell. The poorly defined crystal surfaces make the choice of a specific reconstruction difficult. Studies by Duke and Wang on clean II–VI surfaces in high vacuum have established general mechanisms for reconstruction on cleavage faces.[26] A general tendency for a bond length conserving rotation of surface II–VI pairs results in the cation relaxing into the surface while the anion is pushed out of the plane. We retain the character of these relaxations in our simulations by radially translating all surface cations 0.40 Å toward the cylindrical axis of the crystallite. The surface anions are translated outward by 0.20 Å. The magnitude of the relaxation is comparable to that of Duke and Wang[26] and it is chosen to provide the best fit to the experimental data. The average bond length is kept to within ±0.005 Å of the bulk value for consistency with EXAFS experiments which show negligible bond length contractions.[22] Figure 14d shows that agreement with experimental spectra can be improved by the introduction of such surface disorder. The choice of the relaxation is not unique and is not an attempt to define a specific surface structure, rather it is to show that surface disorder is compatible with the experimental X-ray data. We fix the amount of surface disorder to that used for the 20-Å particles above since we do not expect it to be strongly size dependent. Effects of surface disorder become imperceptible as the crystallite size increases (>50 Å).

Figure 15 shows the experimental spectrum of a sample of 37 Å diameter crystallites (~1000 atoms) compared with a simulation for crystallites with a defect density of 1.3 stacking faults per crystallite, an aspect ratio of ~1.3 along the (002) direction, and a relaxed surface. These particles are small enough that surface contributions cannot be completely ignored. All three deviations from ideality are required to properly fit the full spectrum. Each deviation affects the spectrum independently and in different regions. The stacking faults mostly affect the area between $2\theta \sim 30°$ and 50°, the prolate shape affects the peak position of the first diffraction feature at $2\theta \sim 25°$, and the surface disorder affects the shape of the first feature.

(26) (a) Duke, C. B.; Patton, A.; Wang, Y. R.; Stiles, K.; Kahn, A. *Surf. Sci.* **1988**, *197*, 11. (b) Wang, Y. R.; Duke, C. B. *Phys. Rev. B* **1988**, *37*, 6417. (c) Horsky, T. N.; Brandes, G. R.; Canter, K. F.; Duke, C. B.; Paton, A.; Lessor, D. L.; Kahn, A.; Horng, S. F.; Stevens, K.; Stiles, K.; Mills, A. P., Jr. *Phys. Rev. B* **1992**, *46*, 7011.

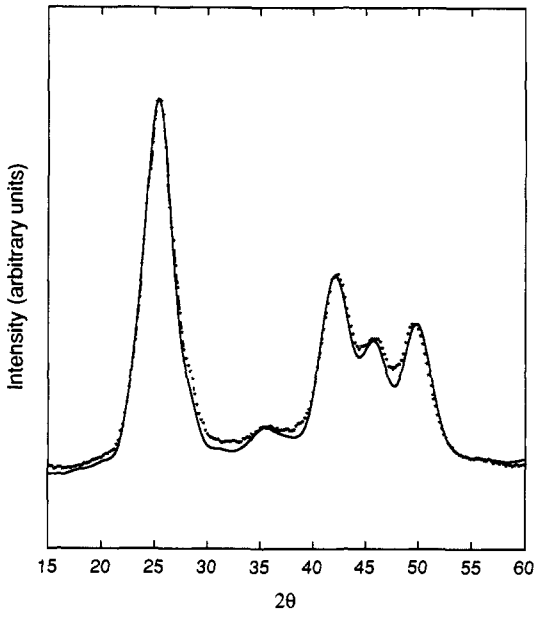

Figure 15. Experimental X-ray powder diffraction spectrum of ~37 Å (~1000 atoms) diameter crystallites (dotted line) compared with a simulated spectrum (solid line) for wurtzite crystallites containing ~1000 atoms with one stacking fault per crystallite in the (002) direction, an aspect ratio of 1.3 along the (002) axis, and a small amount of surface disorder.

In summary, powder X-ray diffraction patterns of a series of CdSe samples can be fit with computer simulations using parameters consistent with TEM and EXAFS investigations. These simulations assume a bulk crystal structure and rely on a small number of parameters (seven) to develop a working description of average crystallite morphology. These parameters are the lattice constant, the amount of thermal disorder (Debye–Waller factor), crystallite size, aspect ratio, stacking fault defect density, the amount of surface disorder, and a constant background correction. As noted above, each parameter affects the powder pattern independently and in a different region, giving a robust fit. Of these seven parameters, two are fixed from TEM and EXAFS data: The lattice constant is fixed at the bulk value (EXAFS) and the crystallite size if taken from TEM measurements. Of the remaining five parameters, four (aspect ratio, surface disorder, background correction, Debye–Waller factor) are fit for one crystallite size and then fixed at that value for the whole series of sizes. As noted, these four parameters are also consistent with independent structural probes. The remaining parameter, the average stacking fault defect density, is allowed to float from size to size. Its value is however relatively constant over the entire series of sizes.

The combination of X-ray studies and TEM imaging yields a description of average CdSe nanocrystallite structure. Strict classification of the structure as purely wurtzite or zincblende is potentially misleading. TEM images of crystallites grown slowly at high temperature provide dimensions of slightly prolate particles and indicate the presence of stacking faults in the (002) direction. Diffraction patterns are consistent with a predominantly wurtzite structure averaging one stacking fault defect every 6–7 planes in the elongated (002) direction. The presence of planar disorder may be important in understanding the influence of structure on the electronic properties and phase stabilities of nanocrystallites. The prolate shape results in a greater coherence length in the (002) direction and provides a potential explanation for the apparent shift in the first diffraction peak without requiring significant lattice contractions or phase transitions. A small amount of surface disorder, consistent with TEM and EXAFS observations, improves agreement between simulated and experimental diffraction spectra but does not uniquely define a surface structure.

IV. Conclusion

A relatively simple route to the synthesis of macroscopic quantities of nearly monodisperse II–VI semiconductor nanocrystallites is presented. The technique allows an entire series of samples, ranging from ~12 to 115 Å in diameter, to be obtained in a single reaction and in macroscopic quantities. The particles produced have uniform size, shape, and surface passivation and show relatively sharp absorption and emission features at room temperature.

The combination of TEM imaging and comparisons of experimental and simulated X-ray diffraction spectra provides a self-consistent description of crystallite structure. These studies highlight the importance of shape and disorder in interpreting experimental results. Average bulk bond lengths and a predominantly hexagonal (wurtzite) crystal structure are found, even in crystallites containing as few as 275 atoms (~20 Å diameter).

The synthetic rationale and systematic structural analysis presented here should be generalizable to the production of a variety of new nanocrystalline materials.

Acknowledgment. We thank Mike Frangillo and Bashir Dabbousi for valuable assistance with the transmission electron microscopy, Peter Nelson for helping set up the computer modeling, and Vicki Colvin for useful discussions. C.B.M. and D.J.N. gratefully acknowledge fellowships from NSERC and NSF, respectively. This research was funded in part by the MIT Center for Materials Science and Engineering (NSF-DMR-90-22933), NSF (DMR-91-57491, CHE-89-14953, and ECS-91-18907), the donors of the Petroleum Research Fund, administered by the American Chemical Society (ACS-PRF-24398-G6), and the Lucille and David Packard Foundation.